General Features of MCSs with the Organization of Multiple Parallel Rainbands in China

PEIYU WANG[a] AND ZHIYONG MENG[a]

[a] Department of Atmospheric and Oceanic Sciences, School of Physics, and China Meteorological Administration Tornado Key Laboratory, Peking University, Beijing, China

(Manuscript received 2 November 2022, in final form 1 June 2023, accepted 7 June 2023)

ABSTRACT: Multiple parallel rainbands (MPRBs) involve the organization of mesoscale convective systems (MCSs) characterized by multiple parallel convective rainbands, which may produce high rainfall accumulation. A total of 178 MPRBs were identified from 2016 to 2020 in China, which were classified into the initiation type (~40%), where rainbands initiate individually, and differentiation type (~60%), where rainbands form through the splitting of large rainbands or merging of smaller cells. Results showed that the occurrence frequency of MPRBs peaks in July with a midnight major peak and a morning minor peak. The highest occurrence frequency is observed in the northern Beibu Gulf and its coastal areas, with minor high frequencies in Guangdong, northern Jiangxi, and southern Shandong provinces, typically in a southwesterly low-level jet to the west of the subtropical high. MPRBs mainly contain 3–4 rainbands with a spacing distance of 30–50 km and an orientation generally consistent with the direction of 850-hPa winds and 0–1-km vertical wind shear. MPRBs generally move slower than that of squall lines in East China ranging from 4 to 8 m s^{-1} with 16% being quasi-stationary, which is mainly due to the occurrence of band back building mainly associated with cold pool. Most MPRBs have training effects with band training as the dominant mode. Because of the band training effect and slower movement of MPRBs mainly due to band back building, 71% of MPRBs are associated with enhanced maximum hourly rainfall. Rainfall severity may be alleviated somewhat by the generally short duration of MPRBs with 78% being shorter than 2 h.

SIGNIFICANCE STATEMENT: The purpose of this study is to document the general features of mesoscale convective systems (MCSs) with a specific organization of multiple parallel rainbands (MPRBs). MCSs with this unique organization tend to produce extremely heavy rainfall partly due to the training of multiple rainbands as well as their slow movement because of back building. The organization pattern of MPRBs was previously found in a case study. The possible formation mechanism was also previously examined based on case studies. As a complement to these studies, this work aims to reveal the temporal and spatial distributions, movement and duration, morphology, precipitation patterns, and environmental features of MPRBs in China based on statistics using 5-yr radar reflectivity data.

KEYWORDS: Convection lines; Squall lines; Mesoscale systems; Morphology; Rainbands; Rainfall

1. Introduction

A mesoscale convective system (MCS) is a cloud system occurring in connection with an ensemble of thunderstorms and produces a contiguous precipitation area on the order of 100 km or more at the horizontal scale along at least one direction (Houze et al. 1989; Laing and Fritsch 1997; Houze 2018). Severe weather associated with MCSs is closely related to their organizational modes.

According to the different arrangements of convective and stratiform rainfall regions, various organizational modes have been identified. Parker and Johnson (2000) proposed three organizational forms of linear convection systems, including trailing stratiform precipitation (TS), leading stratiform precipitation (LS), and parallel stratiform precipitation (PS). Gallus et al. (2008) divided convective storms occurring in 10 central states of the United States into nonlinear systems (NL), three types of cellular convection systems, including isolated cells (IC), clusters of cells (CC), broken lines (BL), and five types of linear systems, including squall lines with no stratiform precipitation (NS), TS, PS, LS, and bow echoes (BE). They found that linear systems could generate more severe weather than NL systems. Zheng et al. (2013) divided MCSs in East China into seven predominant morphologies, including one NL mode and six linear modes. They examined the frequency of different types of severe weather conditions under different organization patterns and found significant differences in MCS-produced severe weather between dry and moist environments. Short-term intense precipitation more frequently occurred in moist environments, while high winds and hail tended to occur in dry environments. Embedded lines (EL) and PS exhibited the highest frequency of short-term intense precipitation because they usually develop in moist environments.

Luo et al. (2014) proposed a new organization of MCSs that tends to produce extremely heavy rainfall when they examined an extreme-rain-producing MCS in East China. Under this type of organization, the MCS contains multiple parallel rainbands (MPRBs) (e.g., Fig. 1a). Because the convection cells and the rainbands are different along the direction of motion and the spatial scale, there are two types of training effects in an MCS containing MPRBs. One is that the convective cells move along individual rainbands, which is referred to as echo training, and the other is that the parallel

Corresponding author: Zhiyong Meng, zymeng@pku.edu.cn

DOI: 10.1175/MWR-D-22-0304.1

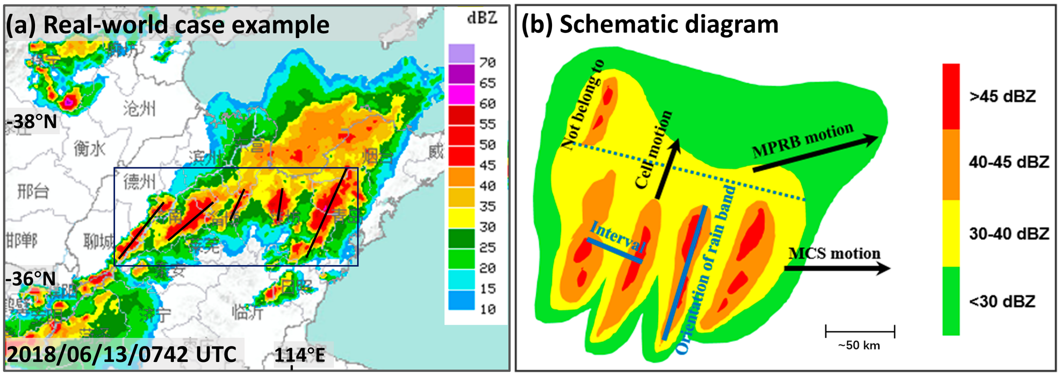

FIG. 1. (a) Real-world case and (b) a schematic diagram of MPRBs.

rainbands move along the direction of movement of the MCS, which is denoted as band training. Following Luo et al. (2014), MPRB cases were also observed in South China (Wang et al. 2014; Liu et al. 2018; Li et al. 2021). Possibly due to the unique double training effect, MPRBs tend to produce extremely heavy rainfall. The MPRB case examined by Luo et al. (2014) caused 298 mm of accumulated rainfall in East China on 8 July 2007.

Echo training has been widely known as one organization mode that tends to produce heavy rainfall, in which many intense convective cells pass in succession across the same location. Schumacher and Johnson (2005) found that the training line–adjoining stratiform (TL/AS) and back building/quasi-stationary (BB) modes were the two most frequent modes among 116 extreme rainfall events from 1999 to 2001 east of the Rocky Mountains in the United States due to echo training effect. An echo training effect on 10 June 2000, caused a severe flash flooding event in northeastern Spain and resulted in damage amounting to over 65 million Euros and five fatalities (Rigo and Llasat 2005; Martín et al. 2007). Echo training effects have also caused severe flash flooding from North to South China. For examples, an echo training effect occurring in Inner Mongolia on 18 July 2018, produced heavy rainfall resulting in 5 deaths and 2 missing persons (Zhang et al. 2020). An MCS with the echo training effect resulted in 426-mm accumulated rainfall and caused 79 fatalities in Beijing on 21 July 2012. An MCS with the echo training effect produced 274 mm of accumulated rain in Chuzhou, Anhui Province on 4 July 2003 (Zhang and Zhang 2012). Relative to TL/ASs or BBs with pure echo training, whether MPRBs generally have a large potential in producing heavy rainfall with double training effect remains unknown.

In recent years, case studies have been considered examining the formation mechanism of the MPRB structure in coastal South China. Wang et al. (2014) examined an MPRB process on 10 May 2013, and they proposed that the lifting of warm air by a gust front played a major role. Liu et al. (2018) found that the rapid splitting and reestablishment (RSRE) of rainbands led to the formation of an MPRB on 11 May 2014, in South China. These two MCSs with MPRBs all produced extreme rainfall of 451 mm in coastal South China. Wang et al. (2021) emphasized that terrain played an important role in the formation of MPRBs especially in the number and location of rainbands of MPRBs by increasing the nonuniformity in the interaction between warm southerly flow and cold outflow. However, the general features of the spatial and temporal distributions of MCSs with MPRBs and their formation environment in China remain unknown.

The goal of this study is to document the various morphologies of MCSs with MPRBs observed in China from 2016 to 2020, their temporal and spatial distributions, movement and duration, associated precipitation patterns and environmental features. A database and methodology are introduced in section 2. Section 3 presents the statistical results. A summary is given in section 4.

2. Data and method

a. Data

This study focused on all MCSs with MPRB organization in China during the period from 2016 to 2020. A regional radar mosaic of basic reflectivities provided by the China Meteorological Administration was used to identify the initiation and evolution of MCSs and the formation of MPRBs. The radar mosaic of basic reflectivities is an optimal selection from the lowest three elevation angles (i.e., 0.5°, 1.5°, and 2.4°) (Bai et al. 2020b), which is also called a "terrain-based hybrid scan" (Fulton et al. 1998). In particular, the larger value from 1.5° to 2.4° elevation angles is used if the ratio of reflectivity area from 1.5° over 0.5° elevation angles is lower than certain criteria. Otherwise, the larger value from 0.5° to 1.5° elevation angles is used. This method is to avoid large area of super refraction at the lowest elevation angle and/or to compensate beam blockage at lower elevation angles. The basic reflectivity had a spatial resolution of 1 km and a temporal resolution of 6 min from 2016 to 2020, except that part of the data in 2016 had a temporal resolution of 10 min. The number of radars over the whole mainland China was 199 in 2016, 206 in 2017, 214 in 2018, 224 in 2019, and 227 in 2020. The radar coverage in eastern China is quite dense, with an average distance of ~200 km. The European Centre for Medium-Range Weather Forecasts (ECMWF) ERA5 dataset (Hersbach et al. 2018) with a resolution of 0.25° × 0.25° was used to examine the environmental features of MPRBs. Hourly rainfall observations

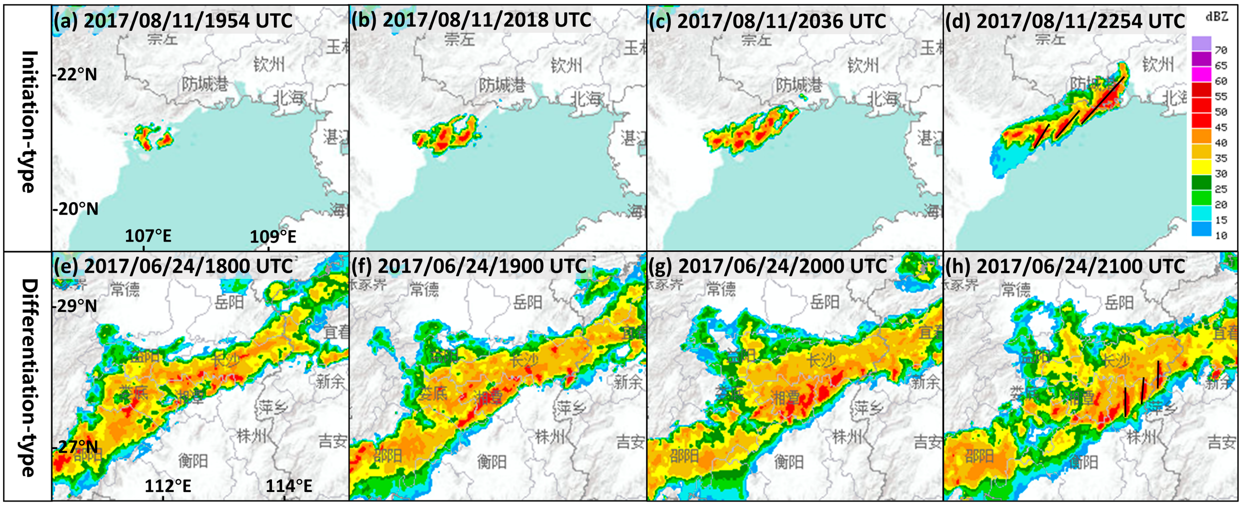

FIG. 2. Examples of the (a)–(d) initiation-type and (e)–(h) differentiation-type MPRBs.

retrieved from rain gauges were provided by the China Meteorological Administration.

b. Identification of MPRBs

We identify MPRBs following three sequential steps. First, a convective system needs to meet the criteria of an MCS. MCS is defined when the area of radar reflectivities above 40 dBZ in the radar mosaic persists at least 3 h and the area with reflectivities above 30 dBZ longer than 100 km along at least one direction persists for longer than 3 h. Reflectivity-based criteria for MCS has been widely determined as groups of convective echoes with extents greater than 100 km and durations greater than 3 h. In studies using composite radar mosaic (e.g., Parker and Johnson 2000; Schumacher and Johnson 2005; He et al. 2017), 40 dBZ and beyond have been used to represent convective echoes. Considering our study uses radar mosaics of reflectivities at one single elevation angle rather than maximum value in vertical direction, we require the area with reflectivities above 30 dBZ longer than 100 km along at least one direction and the sustaining of 40 dBZ value persists for longer than 3 h.

Second, rainbands in the identified MCS are determined when the area with a continuous radar reflectivity above 40 dBZ exhibits a length of more than 30 km with a long-axis to short-axis ratio greater than 2. A rainband has been qualitatively defined as a band area with reflectivities of 35 dBZ and beyond (Luo et al. 2014; Wang et al. 2014; Liu et al. 2018). To guarantee it is a convective rainband, we require that the 40 dBZ area has a band shape, which is defined as a length of more than 30 km with a long-axis to short-axis ratio greater than 2.

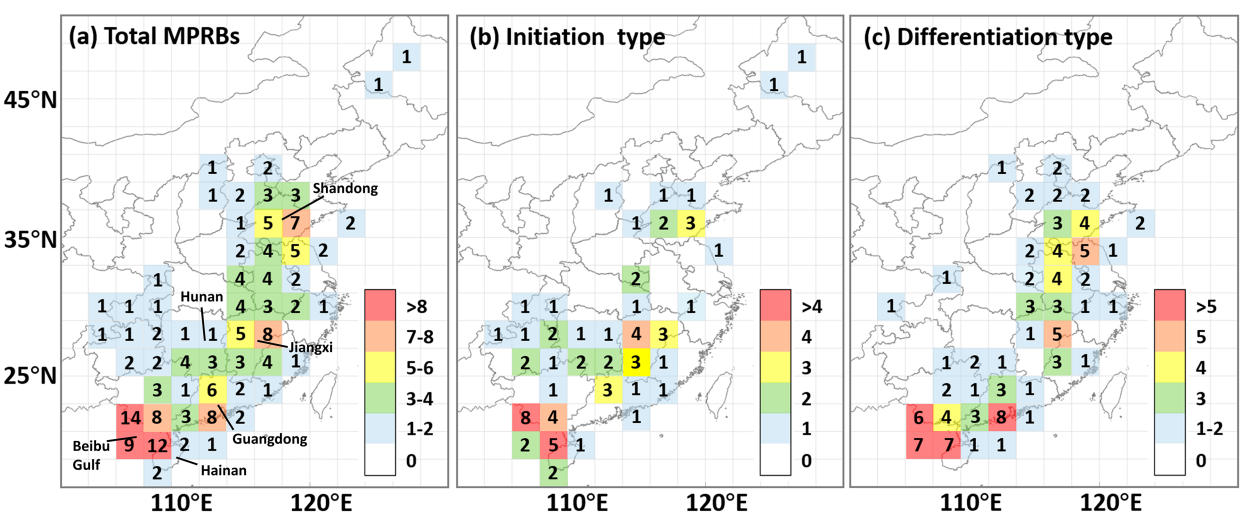

FIG. 3. Geographical distribution of the frequency of the (a) total, (b) initiation-type, and (c) differentiation-type MPRBs. The numbers indicate the frequency of MPRBs in the corresponding data square spanning a 2° × 2° area and represent the number of times that the centroids of the MPRBs lie within the grid square at the corresponding formation times.

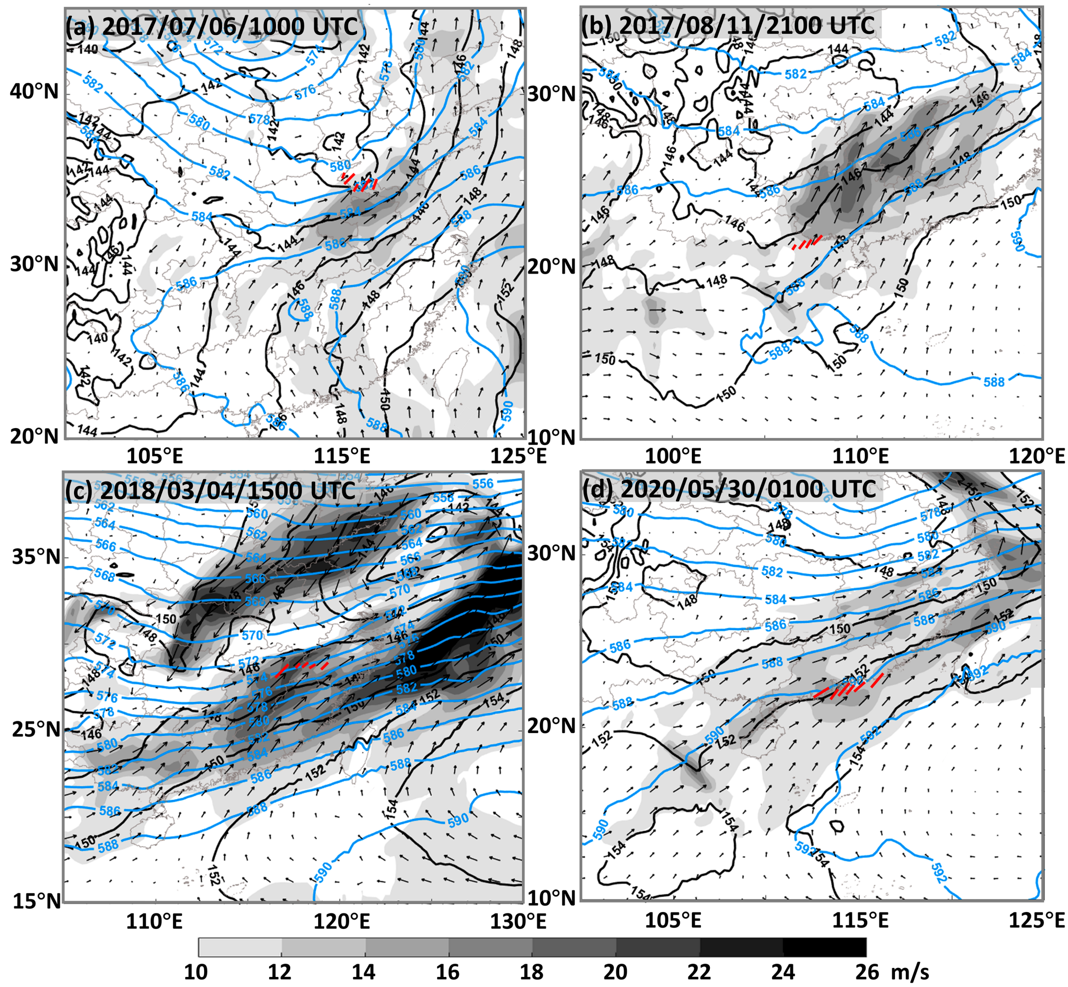

FIG. 4. ERA-5 analyses of the four typical cases, including the 500-hPa geopotential height (blue contour, every 20 gpm), 850-hPa geopotential height (black contour, every 20 gpm), 850-hPa wind (black arrows; m s^{-1}), and velocity (shading; m s^{-1}) at (a) 1000 UTC 6 Jul 2017, (b) 2100 UTC 11 Aug 2017, (c) 1500 UTC 4 Mar 2018, and (d) 0100 UTC 30 May 2020. The red solid lines indicate the rainbands of the respective MPRB cases.

Third, based on the identified rainbands in an MCS, MPRBs are defined when 1) at least three rainbands simultaneously exist for more than 20 min; 2) the angles between the long axes of all rainbands are less than 45° to guarantee that rainbands are approximately parallel; and 3) On the entire major axis of any rainband within the examined MPRB, there exists at least one point through which a straight line parallel to the minor axis of the rainband intersects with other rainbands to guarantee that the rainbands are not too far apart in the direction perpendicular to the long axis of its parent MPRB (Fig. 1b). This condition can be judged by finding at least one line parallel to the minor axis of the rainband intersecting with other rainbands. An example of a rainband that does not belong to the MPRB is given on the up left corner of Fig. 1b where even the straight line parallel to the minor axis at the southern end of the rainband does not intersect with other rainbands. Since MPRB was not defined in a quantitative way in previous papers (Luo et al. 2014; Wang et al. 2014; Liu et al. 2018), the criteria used in our statistics are somewhat empirical.

MPRB is different from wavelike convective bands associated with gravity waves, or horizontal convective rolls, or undular bores. As defined above, MPRB is one organization pattern of MCS. It is a deep moist convection system that develops in an environment with sufficient instability and moisture and acquires at least certain area of 40 dBZ for a certain period of time. However, the other three types of bands are mainly made up of fair weather cumuli or clear-air thermals. Wavelike convective bands associated with gravity waves occur mainly in a stable environment with reflectivities generally lower than 35 dBZ and below 500 hPa with the vertical velocity generally lower than 0.5 m s^{-1} (e.g., Du and Zhang 2019). Horizontal convective rolls are mainly constrained within the boundary layer, displaying as shallow cloud streets on visible satellite imagery and fine lines of <10-dBZ reflectivities on radar. Undular bore usually displays

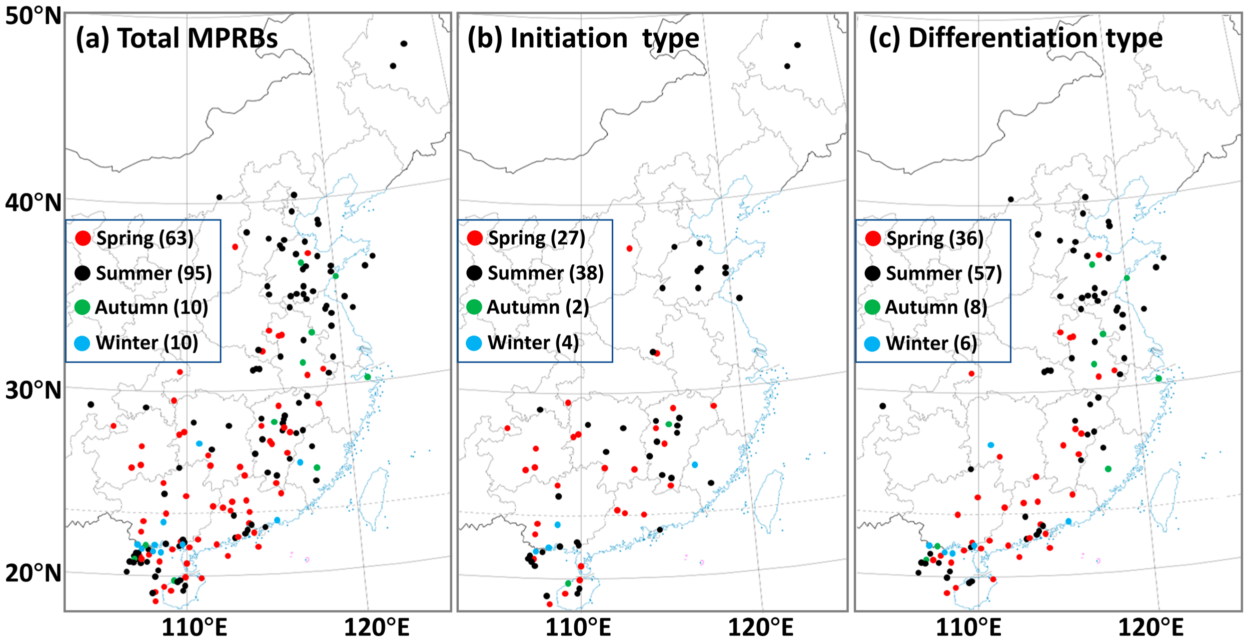

FIG. 5. Seasonal distributions of the (a) total, (b) initiation-type, and (c) differentiation-type MPRBs. The number of MPRBs during the different seasons is given in parentheses.

as a smooth band of shallow cloud along the leading edge reminiscent of a gust-front arc cloud, and other interface bands along the wave crests of the following lower-amplitude waves. These three processes may initiate deep moist convection to form MPRBs. Horizontal convective rolls and undular bores are not likely to be mixed with MPRBs in identification according to our criteria though they may have similar length or spacing distance. There might be a small percentage of wavelike convective bands associated with gravity waves satisfying our criteria of MPRBs.

c. *Classification of MPRBs*

We classify the MPRBs in terms of their formation methods, which are most distinct in two types, namely, the initiation type and the differentiation type (Fig. 2). These two formation mechanisms have been proposed by Wang et al. (2014) and Liu et al. (2018). Initiation-type MPRBs occur at the initiation stage of their parent MCSs, where most rainbands initiate and develop individually without obvious interaction (e.g., Figs. 2a–d). Differentiation-type MPRBs mainly form through the splitting of large rainbands or merging of isolated cells (e.g., Figs. 2e–h). Specifically, one large rainband or convective region splits or turns into two or more rainbands, and/or isolated convection cells merge to form rainbands. Most differentiation-type MPRBs form at the intensive and/or mature stages of their parent MCSs.

d. *Movement of MPRBs and rainbands*

The movement of MPRB is defined using the center of the MPRB at the beginning and ending times of MPRB duration. The center of MPRB is defined as the center of the quadrilateral formed by the two outermost rainbands. Speed of MPRB is the distance between the centers of the MPRB at the beginning and ending times of MPRB duration divided by the duration of the MPRB.

The movement of rainbands is defined using the strongest rainband at the beginning time of the MPRB with the distance between the centers of this rainband at the beginning and ending times of the MPRB or the time when the rainband no longer fits rainband definition depending on which occurs first, divided by the duration between the two times as defined above. The average spacing distance of rainbands of MPRBs is calculated at the centers of the rainbands in the direction of MPRB movement at the moment of MPRB formation.

e. *Training effects*

Echo training is defined when many intense convective cells pass in succession across the same location. To meet this definition, we require that the angle between the orientation and movement of the rainband is less than 20° based on Doswell et al. (1996). Band training is defined when many intense rainbands pass in succession across the same location. To meet this definition, we require that at least one straight line can be drawn connecting all the rainbands of an MPRB with an angle from the direction of the MPRB movement of less than 20°.

f. *Maximum 1-h precipitation during the MPRB period*

During the entire duration of an MCS, if the MPRB duration exceeds 20 min within a certain hour, this hour is counted as the MPRB hour, while other hours are categorized into the non-MPRB period. For each MPRB hour, the 1-h accumulated rainfall is calculated over the rainfall stations located in a rectangular area (Fig. 1a) covering all MPRBs during this particular MPRB hour. The maximum 1-h rainfall within all

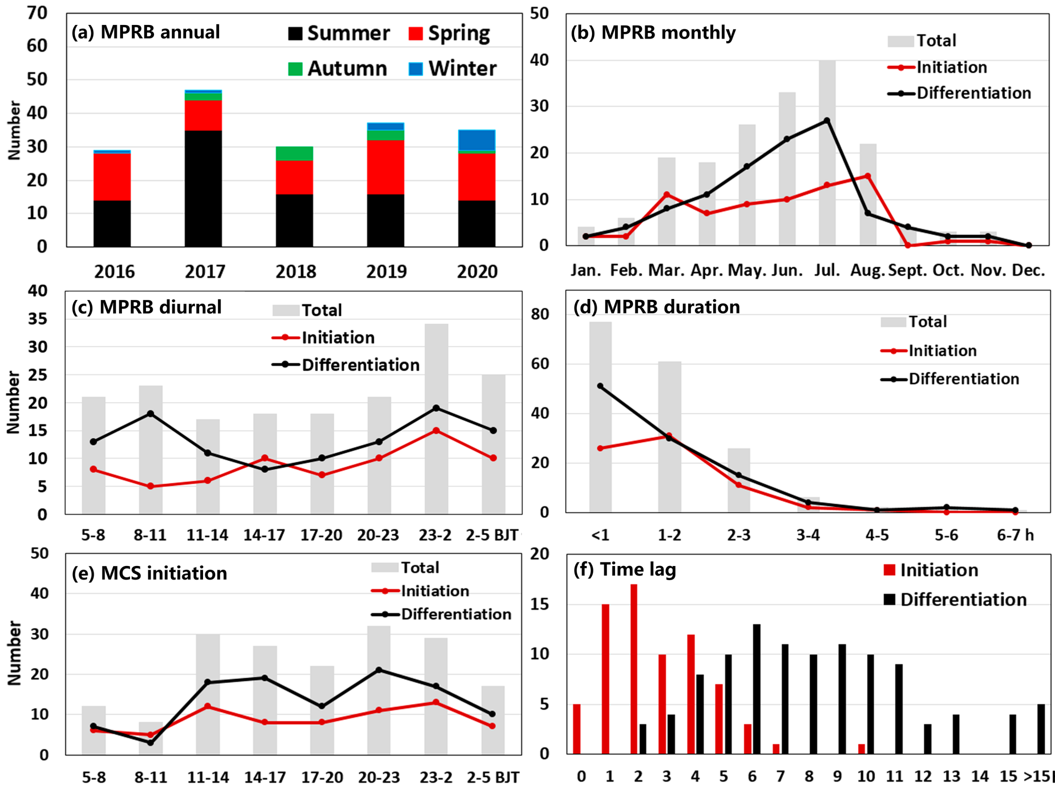

FIG. 6. Frequency of MPRBs by (a) year, (b) month, (c) day, and (d) duration. Also shown are the (e) frequency of the initiation times of parent MCSs of MPRBs and (f) the time lag of the formation time of MPRBs from the initiation time of their parent MCSs. The total, initiation-type, and differentiation-type MPRBs are denoted in gray, red and black colors in (b)–(f).

MPRB hours is adopted to represent the 1-h maximum precipitation during the MPRB period.

3. Results

a. Spatial distribution

A total of 178 MPRB cases during the five-year period from 2016 to 2020 were identified using the thresholds given in section 2b, including 107 differentiation-type cases and 71 initiation-type cases. MPRBs attain the highest frequency in the northern Beibu Gulf and its coastal area, and some minor high-frequency areas occur in Guangdong, northern Jiangxi, and southern Shandong provinces (Fig. 3a). The differentiation type exhibits a distribution similar to that of the total MPRBs but with the highest frequency in the southern coastal area of Guangdong Province (Fig. 3c), while the initiation type exhibits the highest occurrence frequency in the northern Beibu Gulf and its coastal area (Fig. 3b), which is consistent with the high frequency of convection initiation in this region (Bai et al. 2020a).

Although most of the high frequency areas are accompanied by complex topography, the locations of MPRBs are not apparently terrain locked. Background circulations may have played an important role in the formation of high-frequency areas. Synoptic environment of typical cases in the four high-frequency regions of MPRBs are given in Fig. 4. All four MPRBs occurred in southwesterly flow to the west of the subtropical high and in front of a westerly trough at 500 hPa, and in a southwesterly low-level jet (LLJ) at 850 hPa. Zhang and Meng (2019) demonstrated that there is a high frequency center of southwesterly boundary LLJ at ~925 hPa over Beibu Gulf and the coastal area of Guangdong Province, and a synoptic LLJ at ~800 hPa over South China. The high frequency of LLJ may have contributed to the top two high-frequency centers of MPRBs at Beibu Gulf and the Pearl River Delta region (e.g., Figs. 4b,d) with the strong southwesterly wind at 925 hPa or 800 hPa advecting the initiated cells northeastward. Most cases in the high-frequency area of southern Shandong have similar background flow features, where MPRBs are mostly located in LLJs between the subtropical high in the western Pacific Ocean and a more apparent westerly trough (e.g., Fig. 4a). This configuration facilitates sufficient water vapor and strong vertical wind shear. The high frequency in northern Jiangxi mostly featured convergence of warm southwesterly jet with cold northeasterly wind with not only strong vertical shear but also horizontal wind shear (e.g., Fig. 4c). In fact, approximately one-half of the MPRBs in the whole database formed in an environment with an apparent horizontal wind shift. Terrain may have some influence on the behavior of MPRBs as demonstrated in the case study by Wang et al. (2021). Statistically, how decisive terrain is in the formation of MPRBs awaits numerical experiments on many

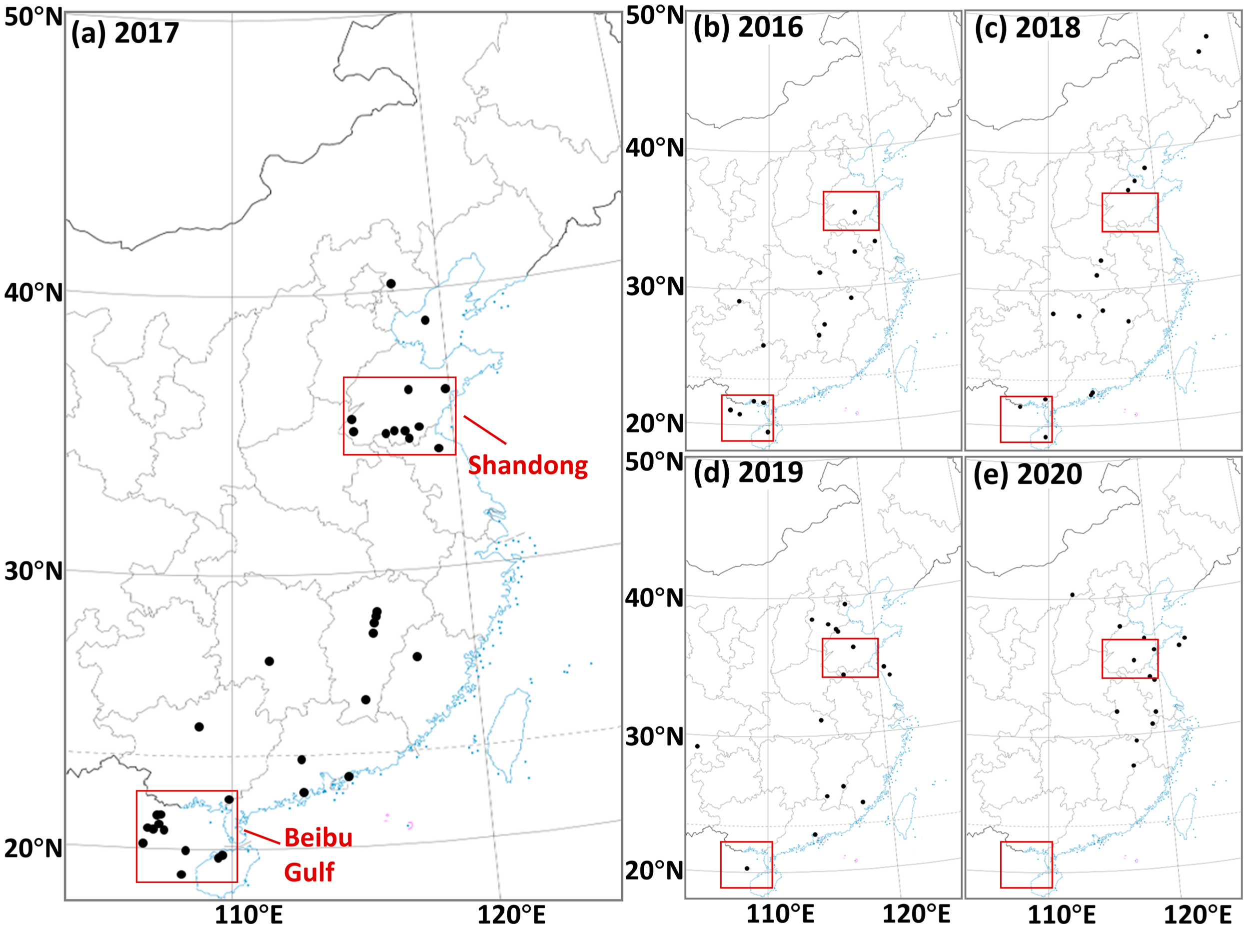

FIG. 7. Yearly variation of MPRBs for summer season.

more cases. Terrain may have some influence on the behavior of MPRBs as demonstrated in the case study by Wang et al. (2021). Statistically, we did not find dominant collocations between MPRBs with mountain valleys or gaps in most cases in all the four high frequency regions in Guangdong, Guangxi, Jiangxi and Shandong provinces.

Similar to ordinary MCSs, MPRBs also exhibit latitudinal propagation with seasonal change. MPRBs mainly form south of 30°N in spring (March, April, and May), from 30° to 40°N as well as in the Beibu Gulf in summer (June, July, and August) and the Beibu Gulf in winter (Fig. 5a). No apparent differences in the seasonal variation pattern are found between these two types (Figs. 5b,c).

b. *Temporal distribution*

The annual number of MPRBs mainly fluctuates at 30, with the highest value in 2017 (Fig. 6a). The total number of MPRBs in summer of 2017 was twice that in other years. The highest frequency of MPRBs in summer 2017 was mainly concentrated in southern Shandong Province and northern Beibu Gulf (Fig. 7). This was possibly related to the larger area, intensity and more westward extension of western Pacific subtropical high in 2017, which generated the most days of high surface temperature since 1961 (Feng et al. 2018). The unusually strong subtropical high and high surface temperature might have produced stronger LLJ between its northern edge and westerly trough, providing higher instability, vertical shear and moisture, and thus generating more frequent severe convection (e.g., Fig. 4a).

The monthly variation exhibits a bimodal structure with the major peak of 40 cases in July and the minor peak of 19 cases in March (Fig. 6b). The number of MPRBs rapidly drops after July, with less than 4 after September. The major peak is mainly attributed to the differentiation type, which maintains a single-peak pattern with 27 cases in July and quickly drops to 7 in August. The initiation type peaks one month later than the differentiation type, but with a minor peak in March, which is possibly due to the special flow pattern in March in South China. Late March is when large extent of severe convections start to form in South China with the converging of warm southwesterly jet with cold northeasterly wind near 30°N (e.g., Fig. 4c), which mainly contributes to the high frequency center in northern Jiangxi Province (Fig. 3). This flow pattern tends to produce multiple MPRBs. There are only two cases where more than 3 consecutive MPRBs were generated

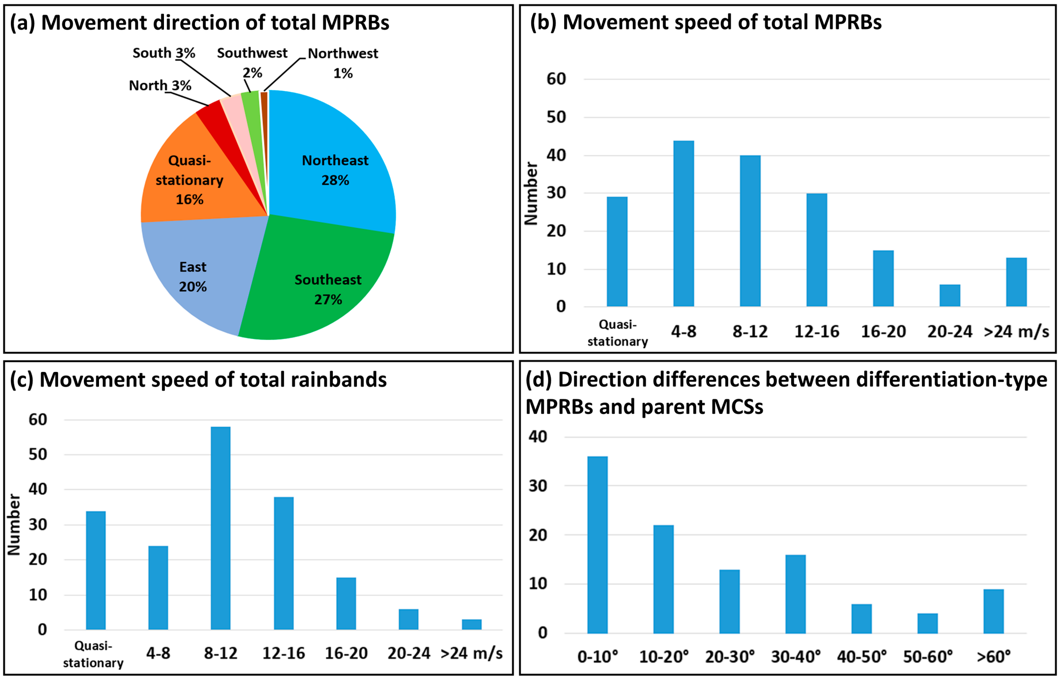

FIG. 8. Distribution of (a) movement direction and (b) speed of total MPRBs, (c) movement speed of total rainbands, and (d) direction differences between differentiation-type MPRBs and parent MCSs.

in one day in the whole database. They both occurred in March near 30°N in 2018 and 2019 in such a flow pattern.

The diurnal variation in the formation times of the MPRBs also exhibits a double-peak structure (Fig. 6c). The major peak occurs at midnight from 2300 to 0200 BJT (BJT = UTC + 8 h), and the minor peak occurs in the morning from 0800 to 1100 BJT. Similar to the total cases, the differentiation type shows two peaks during the same time periods with quite close frequencies. The initiation type exhibits a major midnight peak similar to that of the total cases but with a minor peak in the afternoon from 1400 to 1700 BJT. The differences in the minor peaks of the two types of MPRBs are possibly due to their different time lags of MPRB formation from the initiation time of their parent MCSs. The initiation times of the parent MCSs are similar between the two types of MPRBs (Fig. 6e). However, the differentiation type has a time lag of 5–11 h (Fig. 6f), so that MCSs initiated in the late afternoon are more likely to form MPRBs at midnight and those initiated at night are more likely to form MPRBs in the morning. For the initiation type MPRBs, the lag time is much shorter with the peak of 1–2 h, so that their peaks of formation time are generally overlapped with the initiation times of MCSs in the afternoon and at midnight.

c. *Movement and duration*

Affected by westerlies, most MPRBs have an eastward component of movement. There are 75% of the identified MPRBs that move southeastward, northeastward and eastward (Fig. 8a). The differentiation type MPRBs mostly move in a direction quite similar to that of their parent MCSs (Fig. 8d).

Most MPRBs move at speeds below 16 m s^{-1}, with the highest frequency of MPRBs from 4 to 8 m s^{-1} (Fig. 8b). In particular, quasi-stationary MPRBs, which are defined when the velocity at the center of the MPRBs is lower than 4 m s^{-1}, account for 16% of the total MPRBs. The average speed of MPRBs is 11.5 m s^{-1}, which is ~3 m s^{-1} lower than that of the squall lines in East China with a frequency peak from 12 to 16 m s^{-1} (Meng et al. 2013). The speed of MPRBs is slightly slower than that of their rainbands. The highest frequency of movement speed of the rainbands is from 8 to 12 m s^{-1}, with average and highest speeds of movement of 9.9 and 29.2 m s^{-1}, respectively (Fig. 8c).

The life cycle of MPRBs is generally short. There are 78% of the total cases lasting no longer than 2 h (Fig. 6d). There are 13 cases lasting longer than 3 h, accounting for 7% of the total cases. The duration of the initiation type is mainly 1–2 h. In contrast, most MPRBs of the differentiation type exhibit a duration largely less than 1 h. This is possibly because the presence of many complex interactions between rainbands and between MPRBs and their parent MCSs may easily alter the structure of MPRBs.

d. *Morphology*

Training effect is an important morphology feature of MPRBs (Luo et al. 2014). Our statistics show that 90% of MPRBs have training effects (Fig. 9a). There are 61% of training cases contributed by differentiation type and 39% by initiation type. Different from the case studies (Luo et al. 2014; Wang et al. 2014) where both echo training and band training were observed, our statistic shows that only 24% of MPRBs

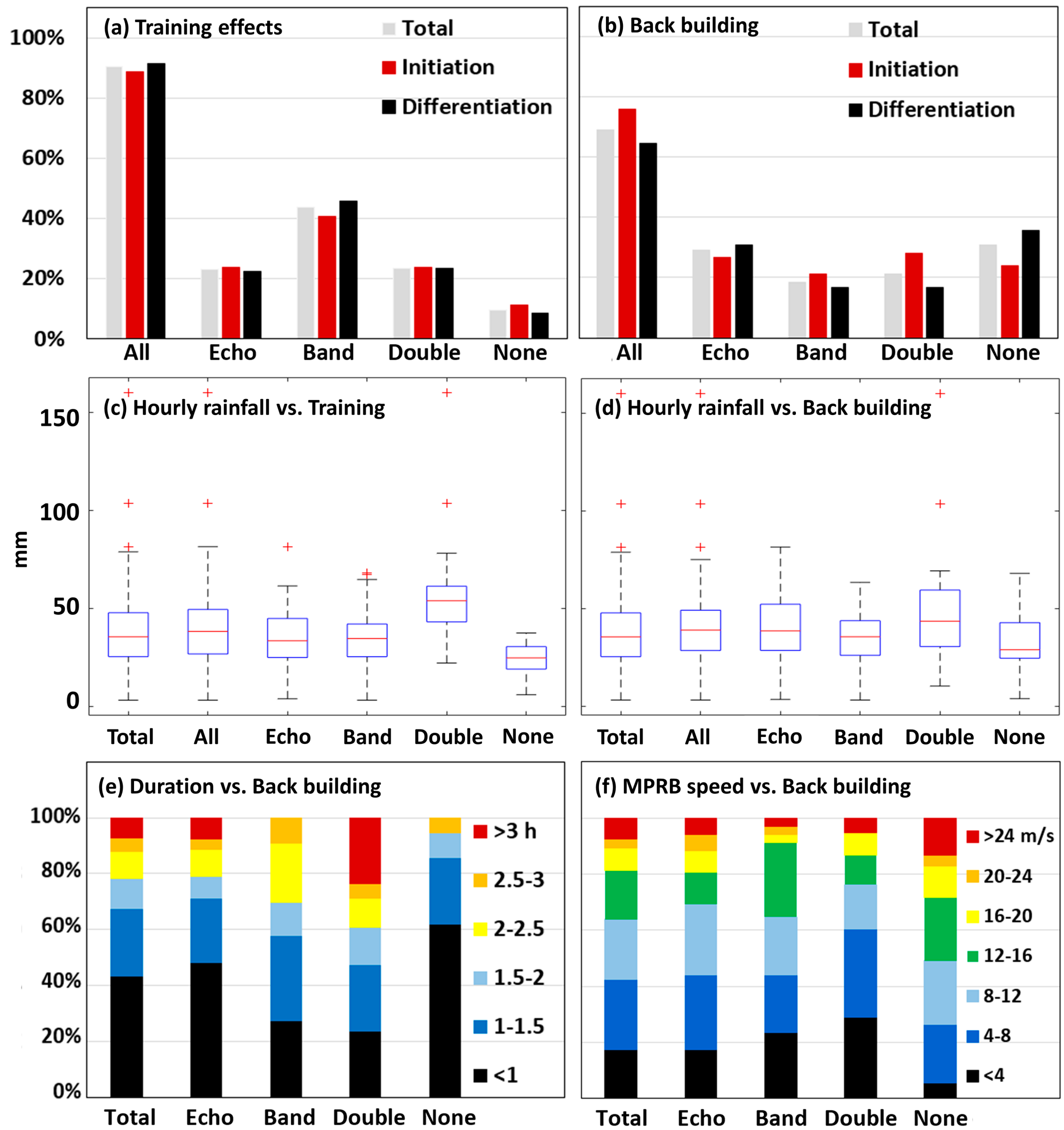

FIG. 9. Proportion of (a) training effects and (b) back building of the total (gray bar), initiation-type (red bar), and differentiation-type (black bar) MPRBs. Also given are the box-and-whisker plots of hourly rainfall (mm) with respect to various (c) training effects and (d) back buildings, the percentages of MPRB (e) duration and (f) speed with respect to various back buildings. In (c) and (d), the percentile extents and corresponding values represent the 25th–75th percentiles for the boxes, the 10th–90th percentiles for the whiskers, and the 50th percentile for the lines in the boxes. The plus symbols indicate outliers beyond the whiskers.

have both training effects. Most cases only have one type of training with 23% of pure echo training and 44% of pure band training. Training effects are more common in the differentiation type than the initiation type. The initiation type has 89% of cases that have training effect with 24%, 41%, and 24% from double training, pure echo training, and pure band training, respectively. In contrast, the differentiation type has 92% of cases that have training effect with 22%, 46%, and 23% from double training, pure echo training, and pure band training, respectively.

Similar to training effects, two types of back building were observed in MPRBs, including echo back building along the rainband and band back building approximately opposite the movement direction of MPRBs. Our statistics show that 69% of MPRBs have back building (Fig. 9b). Same as training effects, most cases only have one type of back building with 29% of pure echo back building and 19% of pure band back building. The differentiation type has echo back building, band and double back buildings at 31%, 17%, and 17%. When compared with the differentiation type, the initiation type has less echo back building at 27%, but more band and double back building at 21% and 28%.

Results show that back building mainly occur at the upstream edge of cold pools of the parent MCSs of MPRBs.

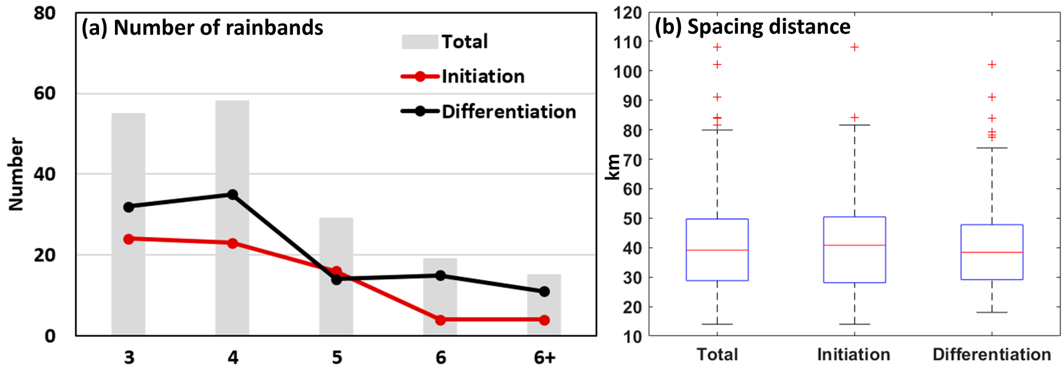

FIG. 10. (a) Number of rainbands of the total (gray bar), initiation-type (red line), and differentiation-type (black line) MPRBs. (b) Box-and-whisker plot of spacing distance of the rainbands. The percentile extents and corresponding values represent the 25th–75th percentiles for the boxes, the 10th–90th percentiles for the whiskers, and the 50th percentile for the lines in the boxes. The plus symbols indicate outliers beyond the whiskers.

Cold pool is defined as a closed region of high temperature gradient around a low-temperature center. Results show that 62% of MPRBs form over or partly over cold pools of their parent MCSs. A similar percentage is observed for the initiation and differentiation types. There are 58% of echo back building and 54% of the band back building occurring at the edge of cold pool. This result shows that cold pools indeed play an important role in the formation of MPRBs through back building, which is consistent with conclusions obtained by case studies of Luo et al. (2014) and Wang et al. (2014).

Back building features of MPRBs have important impact on their duration and movement speed. The duration of MPRBs with band back building is longer than that with echo back building and the duration with double back building is the longest (Fig. 9e). Similarly, the movement speed of MPRBs with band back building is smaller than that with echo back building and the speed with double back building is the smallest (Fig. 9f). Without any kind of back building, MPRBs tend to dissipate quickly and move faster (Figs. 9e,f). This also partly explains why the differentiation type, which has less band and double back building and more non–back building, has more cases with a duration of less than 1 h than the initiation type (Fig. 6d).

The number of rainbands in most identified MPRBs is 3 or 4, with 4 rainbands being the most abundant, accounting for 33% of the total cases (Fig. 10a). Generally, the number of MPRBs decreases with the increasing number of rainbands. Only 19% of MPRBs contain more than five rainbands. On average, the differentiation type contains more rainbands than the initiation type. The average number of rainbands of the differentiation type is five and that of the initiation type is four. Of the differentiation-type MPRBs, 24% contain more than five rainbands. The spacing distance of the interval of rainbands is about 30–50 km. The median for the initiation type is slightly higher than the differentiation type (Fig. 10b).

The angles between the orientation of rainbands and the motion direction of their parent MCSs are mainly 30°–100° (Fig. 1b). Only a few number of rainbands orient 0°–30° and 100°–150°. No apparent differences in the angle of the rainbands were found between these two types. The orientation of rainbands in MPRBs is mainly related to environmental wind. There are 62% of the rainbands that are oriented in the same direction as the 850-hPa winds possibly due to the advection impact of 850-hPa winds on the cell movement (e.g., Fig. 4). In particular, 72% of the echo training cases move in the same direction as the 850-hPa winds.

Our statistic also shows that the rainbands in 70% of all MPRBs orient along the same direction as that of either 0–1-, 0–3-, or 0–6-km vertical wind shear (e.g., Fig. 11). This result suggests that MPRBs may have formed in an environment with larger low-level vertical shear. The average 0–6-km vertical wind shear is approximately 15.4 m s^{-1} (Fig. 12), which is higher than the 0–6-km vertical wind shear associated with the squall lines in East China (~10 m s^{-1} for the component perpendicular to the orientation of the squall lines; Meng et al. 2013). Relative to 0–3- or 0–6-km vertical wind shear, a larger percentage of 51% of all MPRBs orient along the direction of 0–1-km wind shear. Because the vorticities associated with the 0–1-km wind shear and cold pool have the same sense where new cells are initiated (e.g., Fig. 13), the formation and orientation of rainbands along the low-level vertical shear is possibly not owning to the RKW theory, which requires opposite sense of vorticity associated with vertical wind shear and cold pool to produce new cell between them on the down shear side of the cold pool. More than one-half of the MPRBs associated with cold pools have a situation similar to that of Fig. 13. The more possible reason is the advection of the stronger wind at 1–3-km layer associated with LLJs to the initiated cells. There may be other reasons that await further numerical experiments to explore in the future.

The organizational modes from which MCSs evolve into MPRBs were also examined. Cellular systems, NL systems, and 8 types of linear organization systems were identified 2 h before the formation of MPRBs according to the definition of Gallus et al. (2008) and Li et al. (2021). In the 178 MPRBs, 36% of cases evolved from linear modes and 46% from NL modes (Fig. 14a). The top three linear modes included TL, TS, and BE, accounting for 12%, 9%, and 6%, respectively, of the total modes.

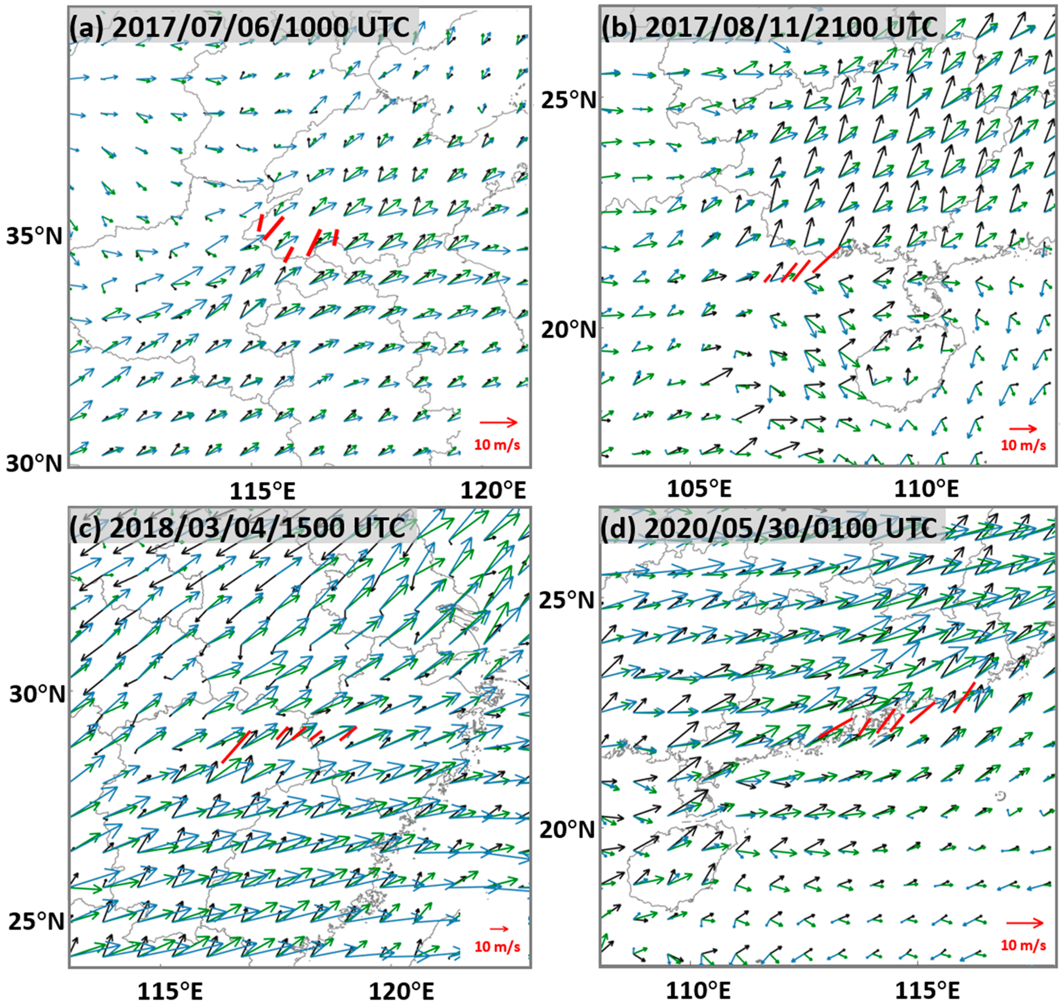

FIG. 11. Diagrams of the 0–1-km (black), 0–3-km (green), and 0–6-km (blue) vertical wind shear in the four typical cases shown in Fig. 4. The red solid lines denote the rainbands in the respective MPRB cases.

The organizational modes from which a given MCS evolves and produces the MPRB structure differ between the initiation and differentiation types. In regard to the initiation type, the cellular mode accounts for the largest proportion at 42%. Linear systems account for 30% of the total modes, while NL modes account for 28% of the total modes. The TS and NS modes are the most frequent among all linear modes, accounting for 7% of all modes and 24% of the total linear modes (Fig. 14b). Among the differentiation-type MPRBs, the NL mode occupies the largest proportion at 57%. The TL mode is the second most abundant of the total modes, accounting for 18%, followed by the TS, BE, NS, and EL modes, accounting for 11%, 6%, 2%, and 2%, respectively, of all modes (Fig. 14c).

e. Precipitation features

The occurrence of MPRBs apparently enhances the hourly rainfall. The results show that the maximum 1-h accumulated rainfall due to MPRBs is 160 mm, with a median value of 39 mm. In 87% of the cases, the maximum 1-h accumulated rainfall reaches 20 mm. The median value is similar between these two types, while the upper quartile of the differentiation type is higher than that of the initiation type (Fig. 15a). Both the maximum and median 1-h accumulated precipitation values of the MPRBs south of 30°N are higher than those of the MPRBs north of 30°N.

A comparison between the rainfall during the MPRB period and that during the adjacent non-MPRB period with the same length of time (the period immediately before the MPRB period plus part of time after the MPRB period if the time before the MPRB is less than the MPRB period) reveals an enhanced effect on the maximum 1-h rainfall in 71% of all cases (Fig. 15b). In particular, 50% of the cases exhibit an increase in the rainfall amount by more than 5 mm, and 33% of the cases exhibit an increase of more than 10 mm. The variation in the hourly rainfall in four cases with an MPRB period longer than 2 h shows that the precipitation during the MPRB period is apparently higher

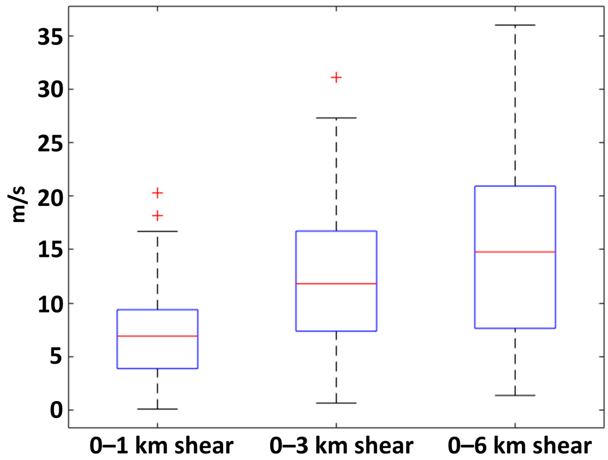

FIG. 12. Box-and-whisker plot of the 0–1-, 0–3-, 0–6-km vertical wind shear of all the MPRB cases. The percentile extents and corresponding values represent the 25th–75th percentiles for the boxes, the 10th–90th percentiles for the whiskers, and the 50th percentile for the lines in the boxes. The plus symbols indicate outliers beyond the whiskers.

and that all MPRB periods contain peak rainfall conditions (Figs. 15c–f).

The rainfall enhancement is the greatest in double training or back building. The cases with band training have a slightly larger median than those of echo training, and the back building is opposite (Figs. 9c,d). Without training effect or back building, the median and high values of hourly rainfall are apparently smaller. The back building features enhance the rainfall mainly through increasing the duration and decreasing the movement speed of MPRBs as discussed in section 3d.

4. Summary

In this work, we performed a survey on the MPRB organizational mode of MCSs in China during the period from 2016 to 2020. A total of 178 MPRB cases were identified based on a radar mosaic of basic reflectivities. These MPRBs were divided into initiation- and differentiation-type MPRBs according to their formation patterns, and nearly two-thirds of the cases were of the differentiation type.

MPRBs attain the highest frequency in the northern Beibu Gulf and its coastal areas, which can be equally attributed to the differentiation and initiation types. Another three minor high-frequency areas are located in Guangdong, northern Jiangxi, and southern Shandong provinces, which are mainly attributed to the differentiation type. The initiation type is the most frequent in the northern Beibu Gulf, while the differentiation type is the most frequent in the southern coastal area of Guangdong Province.

Background circulations rather than terrain impact may have played an important role in the formation of high-frequency areas of MPRBs. Synoptic environments in the four high-frequency regions of MPRBs are featured of southwesterly low-level jet (LLJ) at 850 hPa to the west of the subtropical high and in front of a westerly trough. Approximately one-half of the MPRBs in the whole database form in an environment with an apparent horizontal wind shift. This configuration facilitates sufficient water vapor and strong vertical wind shear and thus strong wind at 1–3 km above the ground to advect initiated cell northeastward.

The occurrence of MPRBs exhibits a major peak in July and a minor peak in March. The peak in July is mainly observed in both the differentiation and initiation types, while the minor peak in March is more related to the initiation type. The diurnal variation in the formation frequency of MPRBs reveals a major peak at midnight (2300–0200 BJT) and a minor peak in the morning (0800–1100 BJT). The major peak could be attributed to both types, while the minor peak is mainly attributable to the differentiation type. The initiation type achieves a minor peak in the afternoon (1400–1700 BJT), while the differentiation type has a minor peak in the morning rather than afternoon. This difference is possibly due to different lag times between formation time of MPRBs and the initiation time of their parent MCSs, which is 5–11 h for the differentiation type and 1–2 h for the initiation type.

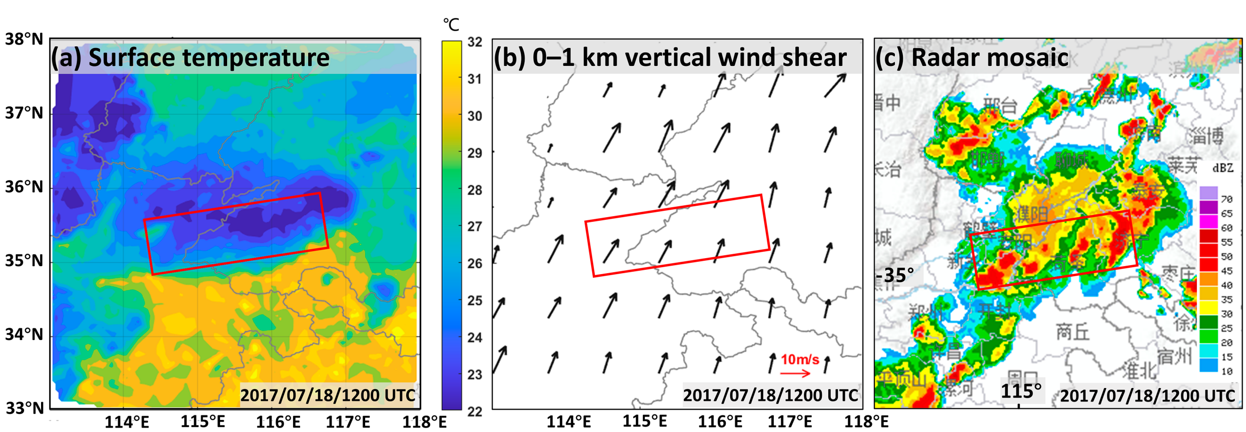

FIG. 13. (a) Surface temperature, (b) 0–1-km vertical wind shear, and (c) radar mosaic of basic reflectivities for an MPRB case at 1200 UTC 18 Jul 2017.

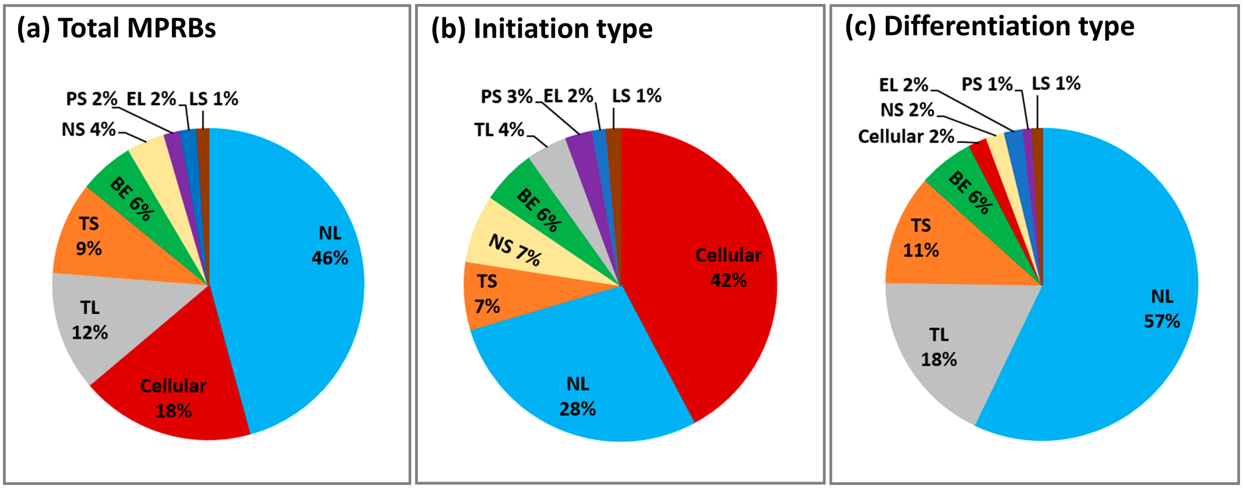

FIG. 14. Pie charts of the organizational transformation of the (a) total, (b) initiation-type, and (c) differentiation-type MPRBs.

MPRBs mainly contain three or four rainbands. On average, the differentiation type contains more rainbands than the initiation type. The spacing distance of rainbands is about 30–50 km. The rainbands are preferentially oriented 30°–100° with respect to the direction of movement of their parent MCSs. The orientation of the rainbands is generally consistent with the wind direction at 850 hPa and the direction of 0–1-km vertical wind shear at the MPRB location, possibly

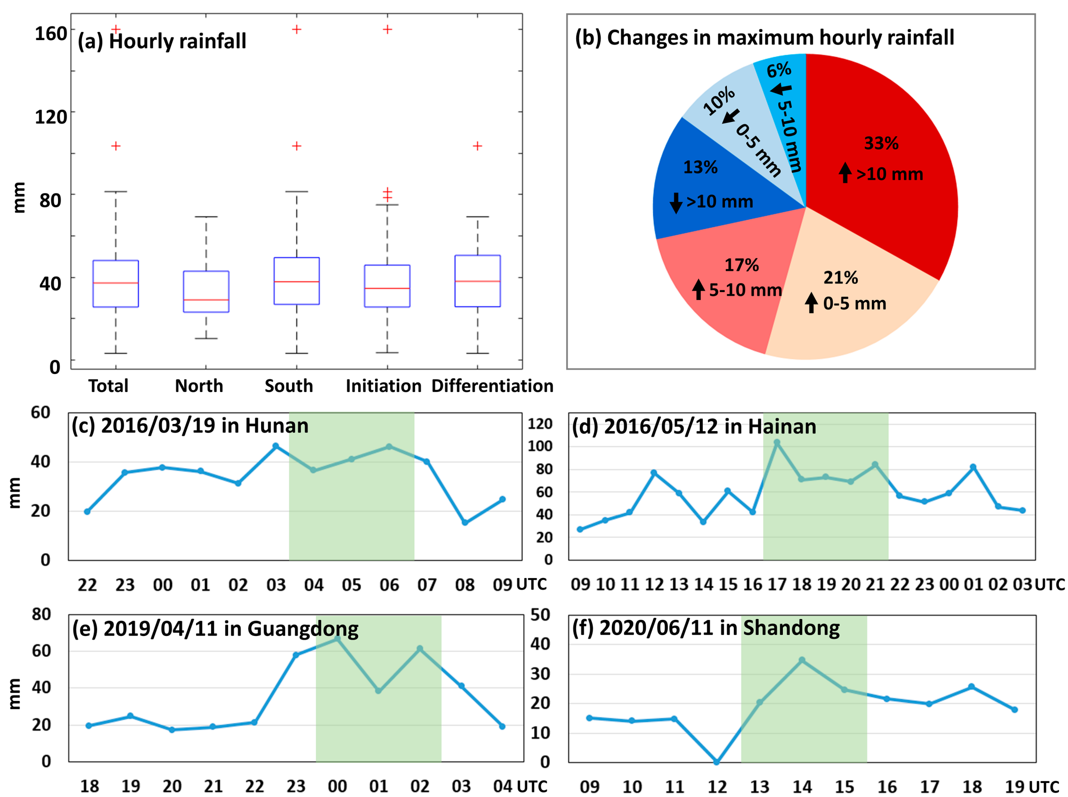

FIG. 15. (a) Box-and-whisker plot of hourly rainfall during the MPRB periods, and (b) changes in the maximum hourly rainfall during the MPRB period from the non-MPRB period, where an upward arrow denotes an increase and a downward arrow denotes a decrease. Also shown are (c)–(f) rainfall variations (blue line) in four MPRB cases with an MPRB period (green shading) longer than 2 h. In (a), the percentile extents and corresponding values represent the 25th–75th percentiles for the boxes, the 10th–90th percentiles for the whiskers, and the 50th percentile for the lines in the boxes. The plus symbols indicate outliers beyond the whiskers. The locations of Hunan and Hainan Provinces for (c) and (d) are given in Fig. 3a.

due to the advection of the strong wind in the layer of 1–3 km above the ground with the existence of LLJ, rather than RKW theory.

MPRBs mainly evolve from NL and cellular modes, accounting for 46% and 18%, respectively, of all modes, followed by the three linear modes of TL, TS, and BE, accounting for 12%, 9%, and 6%, respectively, of all modes. The initiation type mainly evolves from the cellular mode, while the differentiation type mainly evolves from the NL mode.

There are 90% of MPRBs that feature training effects, and only 24% of MPRBs have both training effects. Most cases only have one type of training with 23% of echo training and 44% of band training, which is different from previous case studies. The presence percentage of training effects in the differentiation type is comparable to that in the initiation type. In addition, two different scales of back building were found in MPRBs, which are echo back building and band back building. There are 58% of echo back building and 54% of the band back building mainly occurring at the edge of the cold pool. Back building, especially band back building, apparently prolongs the duration and decreases the movement speed of MPRBs.

Affected by westerlies, 75% of MPRBs move eastward, southeastward and northeastward. The average speed of the MPRBs is 11.5 m s^{-1}. Relative to the general squall lines in East China, the speed of movement of the MPRBs is slightly lower with 16% of quasi-stationary cases possibly due to the back building especially band back building features.

Resulting from their slower movement as well as training effects, especially band training effects, MPRBs impose an enhanced effect on precipitation. A comparison of the maximum 1-h rainfall between the MPRB period and non-MPRB period reveals an increase in rainfall in 71% of the cases of MPRBs. Fortunately, the duration of MPRBs is relatively short with 78% of the cases exhibiting a duration less than 2 h, which may have helped alleviate the possibility of severe rainfall accumulation.

Acknowledgments. This work was sponsored by the National Natural Science Foundation of China (Grant 42030604).

Data availability statement. Radar data, surface observations, and hourly rainfall observations retrieved from rain gauges were provided by the National Meteorological Information Center of the China Meteorological Administration (https://data.cma.cn/data/cdcindex/cid/0b9164954813c573.html). The ERA5 data used in this work [Hersbach et al. (2018) for data on pressure levels] are freely available from the Copernicus Data Store (https://cds.climate.copernicus.eu/cdsapp#!/search?type=dataset).

REFERENCES

Bai, L., G. Chen, and L. Huang, 2020a: Convection initiation in monsoon coastal areas (South China). *Geophys. Res. Lett.*, **47**, e2020GL087035, https://doi.org/10.1029/2020GL087035.

——, ——, and ——, 2020b: Image processing of radar mosaics for the climatology of convection initiation in South China. *J. Appl. Meteor. Climatol*, **59**, 65–81, https://doi.org/10.1175/JAMC-D-19-0081.1.

Doswell, C. A., III, H. E. Brooks, and R. A. Maddox, 1996: Flash flood forecasting: An ingredients-based methodology. *Wea. Forecasting*, **11**, 560–581, https://doi.org/10.1175/1520-0434(1996)011<0560:FFFAIB>2.0.CO;2.

Du, Y., and F. Zhang, 2019: Banded convective activity associated with mesoscale gravity waves over southern China. *J. Geophys. Res. Atmos.*, **124**, 1912–1930, https://doi.org/10.1029/2018JD029523.

Feng, A., and Coauthors, 2018: Climatic characteristics and major meteorological events over China in 2017. *Meteor. Mon.*, **44**, 548–555.

Fulton, R. A., J. P. Breidenbach, D.-J. Seo, D. A. Miller, and T. O'Bannon, 1998: The WSR-88D rainfall algorithm. *Wea. Forecasting*, **13**, 377–395, https://doi.org/10.1175/1520-0434(1998)013<0377:TWRA>2.0.CO;2.

Gallus, W. A., Jr., N. A. Snook, and E. V. Johnson, 2008: Spring and summer severe weather reports over the Midwest as a function of convective mode: A preliminary study. *Wea. Forecasting*, **23**, 101–113, https://doi.org/10.1175/2007WAF2006120.1.

He, Z., Q. Zhang, L. Bai, and Z. Meng, 2017: Characteristics of mesoscale convective systems in central East China and their reliance on atmospheric circulation patterns. *Int. J. Climatol.*, **37**, 3276–3290, https://doi.org/10.1002/joc.4917.

Hersbach, H., and Coauthors, 2018: ERA5 hourly data on pressure levels from 1940 to present. Copernicus Climate Change Service (C3S) Climate Data Store (CDS), accessed 10 October 2019, https://doi.org/10.24381/cds.bd0915c6.

Houze, R. A., Jr., 2018: 100 years of research on mesoscale convective systems. *A Century of Progress in Atmospheric and Related Sciences: Celebrating the American Meteorological Society Centennial*, *Meteor. Monogr.*, No. 59, Amer. Meteor. Soc., https://doi.org/10.1175/AMSMONOGRAPHS-D-18-0001.1.

——, S. A. Rutledge, M. I. Biggerstaff, and B. F. Smull, 1989: Interpretation of Doppler-radar displays in midlatitude mesoscale convective systems. *Bull. Amer. Meteor. Soc.*, **70**, 608–619, https://doi.org/10.1175/1520-0477(1989)070<0608:IODWRD>2.0.CO;2.

Laing, A. G., and J. M. Fritsch, 1997: The global population of mesoscale convective complexes. *Quart. J. Roy. Meteor. Soc.*, **123**, 389–405, https://doi.org/10.1002/qj.49712353807.

Li, S., Z. Meng, and N. Wu, 2021: A preliminary study on the organizational modes of mesoscale convective systems associated with warm-sector heavy rainfall in South China. *J. Geophys. Res. Atmos.*, **126**, e2021JD034587, https://doi.org/10.1029/2021JD034587.

Liu, X., Y. Luo, Z. Guan, and D.-L. Zhang, 2018: An extreme rainfall event in coastal South China during SCMREX-2014: Formation and roles of rainband and echo trainings. *J. Geophys. Res. Atmos.*, **123**, 9256–9278, https://doi.org/10.1029/2018JD028418.

Luo, Y., Y. Gong, and D.-L. Zhang, 2014: Initiation and organizational modes of an extreme-rain-producing mesoscale convective system along a mei-yu front in East China. *Mon. Wea. Rev.*, **142**, 203–221, https://doi.org/10.1175/MWR-D-13-00111.1.

Martín, A., R. Romero, V. Homar, A. De Luque, S. Alonso, T. Rigo, and M. C. Llasat, 2007: Sensitivities of a flash flood event over Catalonia: A numerical analysis. *Mon. Wea. Rev.*, **135**, 651–669, https://doi.org/10.1175/MWR3316.1.

Meng, Z., D. Yan, and Y. Zhang, 2013: General features of squall lines in east China. *Mon. Wea. Rev.*, **141**, 1629–1647, https://doi.org/10.1175/MWR-D-12-00208.1.

Parker, M. D., and R. H. Johnson, 2000: Organizational modes of midlatitude mesoscale convective systems. *Mon. Wea. Rev.*, **128**, 3413–3436, https://doi.org/10.1175/1520-0493(2001)129<3413:OMOMMC>2.0.CO;2.

Rigo, T., and M. C. Llasat, 2005: Radar analysis of the life cycle of mesoscale convective systems during the 10 June 2000 event. *Nat. Hazards Earth Syst. Sci.*, **5**, 959–970, https://doi.org/10.5194/nhess-5-959-2005.

Schumacher, R. S., and R. H. Johnson, 2005: Organization and environmental properties of extreme-rain-producing mesoscale convective systems. *Mon. Wea. Rev.*, **133**, 961–976, https://doi.org/10.1175/MWR2899.1.

Wang, H., Y. Luo, and B. J.-D. Jou, 2014: Initiation, maintenance, and properties of convection in an extreme rainfall event during SCMREX: Observational analysis. *J. Geophys. Res. Atmos.*, **119**, 13 206–13 232, https://doi.org/10.1002/2014JD022339.

Wang, Q., Y. Zhang, K. Zhu, Z. Tan, and M. Xue, 2021: A case study of the initiation of parallel convective lines back-building from the south side of a Mei-Yu front over complex terrain. *Adv. Atmos. Sci.*, **38**, 717–736, https://doi.org/10.1007/s00376-020-0216-2.

Zhang, G., Y. Hang, L. Fu, L. Zhang, and F. Bao, 2020: Causes of a torrential rainstorm induced by "train effect" in Hetao area (in Chinese). *Plateau Meteor.*, **39**, 788–795, https://doi.org/10.7522/j.issn.1000-0534.2019.00122.

Zhang, M., and D.-L. Zhang, 2012: Sub-kilometer simulation of a torrential-rain-producing mesoscale convective system in East China. Part I: Model verification and convective organization. *Mon. Wea. Rev.*, **140**, 184–201, https://doi.org/10.1175/MWR-D-11-00029.1.

——, and Z. Meng, 2019: Warm-sector heavy rainfall in southern China and its WRF simulation evaluation: A low-level-jet perspective. *Mon. Wea. Rev.*, **147**, 4461–4480, https://doi.org/10.1175/MWR-D-19-0110.1.

Zheng, L., J. Sun, X. Zhang, and C. Liu, 2013: Organizational modes of mesoscale convective systems. *Wea. Forecasting*, **28**, 1081–1098, https://doi.org/10.1175/WAF-D-12-00088.1.